

Capture and chaotic scattering of a charged particle by magnetic monopole under uniform electric field

Kou Misaki,¹ Naoto Nagaosa^{1,2}

¹*Department of Applied Physics, The University of Tokyo,
Bunkyo, Tokyo 113-8656, Japan*

²*RIKEN Center for Emergent Matter Science (CEMS),
Wako, Saitama 351-0198, Japan*

(Dated: July 13, 2018)

Motivated by the realization of magnetic monopole of Berry curvature by the energy crossing point, we theoretically study the effect of magnetic monopole under a uniform electric field in the semiclassical dynamics, which is relevant to many physical situations such as relaxation through the diabolic point. We found that the competition between the backward scattering by the monopole magnetic field and the acceleration by the electric field leads to the bound state, i.e., capture of a particle near the monopole. Furthermore, the nonlinearity induced by the magnetic monopole leads to the chaotic behavior in the transient dynamics, i.e., the transient chaos. We computed characteristic quantities of the strange saddle which gives rise to the transient chaos, and verified that the abrupt bifurcation occurs as we tune the system parameter toward the parameter region in which the system is solvable.

Introduction.— Since Dirac theoretically pointed out its possible existence by considering the 2π ambiguity of the phase of an electron wavefunction [1], magnetic monopole has attracted wide theoretical interests and appeared in many areas of physics [2–4]. In particular, magnetic monopole of Berry curvature [5] or synthetic gauge field [6, 7] appears both in real [8–10] and momentum [11–14] spaces, and drastically affects the transport property as it modifies the semiclassical equation of motion for the wave packet of particles [15–18].

Actually, the history of magnetic monopole [19–23] dates back to the late 1800s when Darboux and Poincaré theoretically studied the scattering problem of an electron by a magnetic monopole [24, 25]. This problem can be exactly solved because of the conservation of the angular momentum, and exhibits some unusual properties compared to the usual potential scattering [22, 26]. In this paper, we will show that, upon introducing the uniform electric field, the peculiar nature of this scattering problem leads to the chaotic dynamics, i.e., the chaotic scattering [27, 28].

Model.— We numerically study the equation describing the dynamics of a particle under the influence of monopole magnetic field and the uniform electric field:

$$m \frac{d^2 \vec{r}}{dt^2} = f \vec{e}_z + q_m q_e \frac{d\vec{r}}{dt} \times \frac{\vec{r}}{r^3}, \quad (1)$$

where m is the mass of particle, f is the uniform force along z direction, q_m and q_e are the magnetic charge of the monopole sitting at the origin and the electric charge of the particle, respectively. This equation has two conserved quantities, i.e., the energy and the angular momentum along z direction:

$$E = \frac{m}{2} (\dot{\vec{r}})^2 - fz, \quad J_z = m(xy\dot{z} - y\dot{x}z) - q_m q_e \frac{z}{r}, \quad (2)$$

where the second term of J_z comes from the angular momentum of the electromagnetic field. We can utilize J_z conservation to reduce one degree of freedom [26]:

$$\begin{cases} m \frac{d^2 z}{dt^2} = -\frac{\partial U_{\text{eff}}}{\partial z} \\ m \frac{d^2 \rho}{dt^2} = -\frac{\partial U_{\text{eff}}}{\partial \rho}, \end{cases} \quad U_{\text{eff}} := -fz + \frac{\left(J_z + \frac{q_m q_e z}{\sqrt{z^2 + \rho^2}} \right)^2}{2m\rho^2}, \quad (3)$$

where $\rho = \sqrt{x^2 + y^2}$. Now the system is fully characterized by U_{eff} , and the problem reduces to the usual potential scattering. The form of the potential depends on the value of J_z , which is determined from the initial conditions according to Eq. (2). As we can see from the Fig. 1 (a), there exists a potential saddle for particular parameter range of J_z . If we consider the dynamics of the particle starting from the initial position inside the potential pocket bounded by the saddle and the potential walls, the particle bounces back and forth inside the pocket, and eventually goes over the saddle. Therefore, the existence of the saddle and the potential pocket it bounds are the crucial ingredients for this scattering problem. It turns out that the saddle exists for $|J_z| < \sqrt{32/27}|q_m q_e|$ [26], so we concentrate on the dynamics for this range of J_z .

Since the diverging magnetic field leads to the infinite cyclotron frequency, it invalidates the numerical calculation for the trajectory passing near the origin. To avoid this difficulty, we introduce the smeared magnetic charge:

$$\rho(\vec{r}) = \frac{1}{\xi^3 \sqrt{\pi^3}} \int d\vec{R} e^{-\frac{|\vec{r}-\vec{R}|^2}{\xi^2}} q_m \delta(\vec{R}) = \frac{q_m e^{-\frac{r^2}{\xi^2}}}{\xi^3 \sqrt{\pi^3}}. \quad (4)$$

The magnetic field produced by this magnetic charge is the same as the monopole for $r \gg \xi$, and converges to 0 as $r \rightarrow 0$.

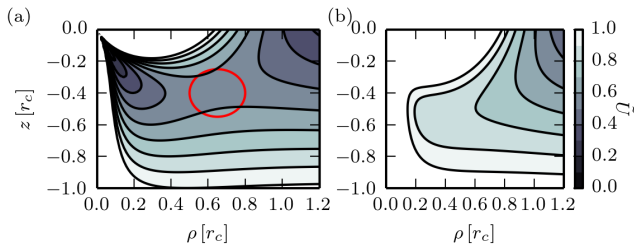


FIG. 1. The distribution of U_{eff} in (ρ, z) plane for (a) $J_z/(q_m q_e) = 0.9$, and (b) $J_z/(q_m q_e) = \sqrt{32/27} + 0.01$. The color represents the potential height $\tilde{U} := U_{\text{eff}}/(f r_c)$, where $r_c := |q_m q_e|^{2/3}/(m f)^{1/3}$, as is shown in the right of (b). We can see the potential saddle as we highlighted with the red circle for (a), while the saddle disappears for (b).

Result.— We performed the numerical calculation of Eq. (1) with the Runge-Kutta method and the implicit Tajima method [29]. We can regard the dynamics described by Eq. (1) as a scattering problem of a charged particle by magnetic monopole. There are two important physical observables: t_{pass} , which is the time it takes for the particle to get out of the scattering region, which we define as $r \leq 2r_c$ ($r_c := |q_m q_e|^{2/3}/(m f)^{1/3}$), and $r_{\text{min}} := \min_t \{r(t)\}$, which determines whether our approximation of the point magnetic charge by the smeared one is good or not. We set the initial velocity to be zero, and vary $z(0) = z_0$ and $x(0) = x_0$ to adjust the incident velocity and the impact parameter, respectively, and set $q_m q_e < 0$. We show the result of the numerical calculation in Fig. 2. For small x_0 (small J_z) and small $|z_0|$ (small energy) region, we observed that t_{pass} becomes larger than the numerically accessible time region. This fact can be understood from the geometry of the effective potential Eq. (3): For this region, the particle cannot escape from the scattering region since the height of the potential saddle is higher than the initial energy. We obtained the analytic expression for the parameter region where this trapping occurs, and verified that the expression matches with the result of the numerical calculation [26]. In addition, we can see the complicated peak structure in the region with small impact parameter, and as is shown in Fig. 3(a), each peak has a fractal structure, and the scattering angle Θ , which is the relative angle between the initial and the final velocity, varies very wildly near this peak structure. We show the dynamics at each hierarchy of the fractal in Fig. 4. We checked the convergence of the peak structure and the small error of conserved quantities, so this peak structure is not an artifact of the finite precision of the numerical calculation. Actually, this fractal structure of t_{pass} is a characteristic feature of the chaotic scattering [27, 28], which is the representative example of the transient chaos [30, 31].

To understand why the chaotic scattering occurs and the multiple peaks for each z_0 is observed, it is convenient

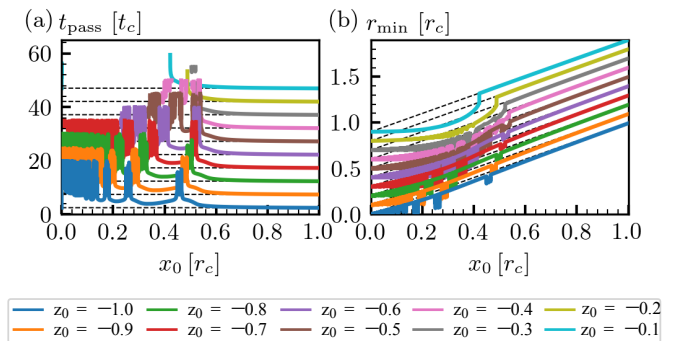


FIG. 2. The plot of the time when the particle get out of the scattering region $r \leq 2r_c$ (t_{pass}) and the minimum value of $r(t)$ ($r_{\text{min}} := \min_t \{r(t)\}$), for the initial position $(x_0, 0, z_0)$. Here $r_c := |q_m q_e|^{2/3}/(m f)^{1/3}$ and $t_c := (m |q_m q_e|)^{1/3}/f^{2/3}$. The numerical calculation was done with an implicit Tajima method. The black dashed line represent the values without the monopole magnetic field. Note that each plot is shown with an offset. The values of the offset are given by the values of the dashed line at $x_0 = 0$. For small x_0 and z_0 , t_{pass} is larger than $t/t_c = 20$, and the plot of t_{pass} at these values are not shown.

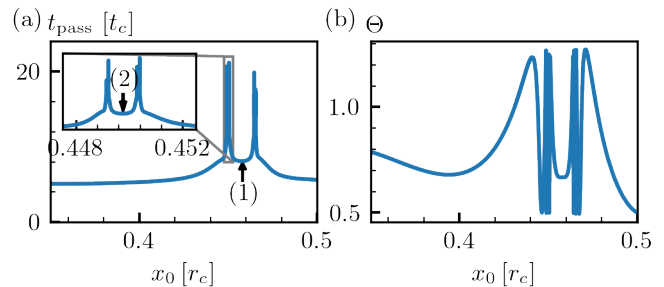


FIG. 3. (a) The peak structure of t_{pass} around $x_0/r_c \cong 0.45$ at $z_0/r_c = -1$. The inset shows the detailed peak structure of the left peak, and we can clearly see the self-similarity of the peak. We showed (1) and (2), which is the parameter point we take for the dynamics shown in Fig. 4. We define the parameter points (n) for all n larger than 2 for finer structures in the same way. (b) The rapid variation of $\Theta := \cos^{-1}(v_z(t_{\text{pass}})/\sqrt{\vec{v}(t_{\text{pass}}) \cdot \vec{v}(t_{\text{pass}})})$ near the fractal peak, which is the characteristic feature of the chaotic scattering [27, 28].

to go back to $f = 0$ limit of Eq. (1). As we mentioned in the introduction, this model is exactly solved. Among some peculiar characteristics, one notable feature is the impact parameter (x_0) dependence of the scattering angle: There are multiple backscattering points (so-called glory scattering) located at $q_e q_m / (m v x_0) = \sqrt{4n^2 - 1}$ ($n = 1, 2, \dots$), where v represents the initial velocity [32, 33]. This is in sharp contrast to the scattering angle in the Rutherford scattering which has a monotonic impact parameter dependence. If we regard each backscattering point as the potential hill, the situation is formally

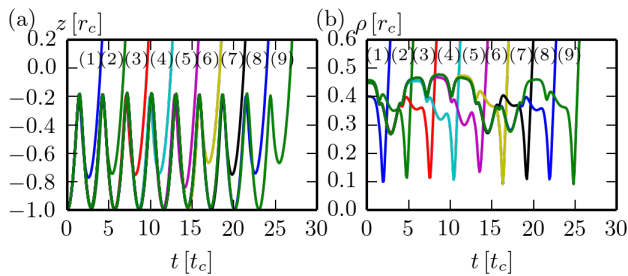


FIG. 4. The plots of (a) $z(t)$ and (b) $\rho(t)$. The value of x_0 at (n) is defined in Fig. 3. We can see the correspondence between the number of the oscillation and the number of the hierarchy.

similar to the scattering problem by multiple scatterer, which is known to exhibit the chaotic behavior at the transient time scale [27, 28]. Moreover, for fixed z_0 there are infinitely many x_0 where the particle is backscattered, and this leads to infinitely many well-separated peak structures [26].

The chaotic scattering can be understood as a consequence of the horseshoe type mapping induced by a intersection of a stable and an unstable manifold of the periodic orbits [34]. This mapping leads to the invariant saddle which has a fractional dimension. The fact that the saddle has a fractal dimension has a drastic consequence on the physical quantities: The dimension of generic crossing of the stable manifold of the saddle and the one parameter family of initial conditions in the phase space becomes fractional. As a result, at each intersection, the time it takes for the particle to get out of the scattering region (t_{pass}) is infinite, so t_{pass} has a peak on the set with a fractional dimension. The dimension of the crossing can be calculated as follows [35]: Our model is the Hamiltonian system with two degrees of freedom (Eq. (3)). Within each energy shell, the dimension of the phase space is three. Noting that Eq. (3) has time reversal symmetry, the dimensions of the stable and the unstable manifold are the same. Since the dimension of the intersection of the two subsets S_1 and S_2 in the d dimensional manifold is given by $D(S_1 \cap S_2) = D(S_1) + D(S_2) - d$, where $D(S)$ represents the dimension of S , and the saddle is given by the intersection of the stable and the unstable manifold, $D(S_{\text{st}}) = (D(S_{\text{sad}}) + 3)/2$, where S_{sad} and S_{st} represent the saddle and the stable manifold of the saddle. Therefore, the dimension of the crossing, which we refer to as the fractal dimension, is given by $d_{\text{fra}} = 1 + D(S_{\text{st}}) - 3 = (D(S_{\text{sad}}) - 1)/2$.

Concerning the dynamics on the saddle, the positivity of the Lyapunov exponent itself does not immediately imply the chaotic behavior, which can be quantitatively understood from the following Kantz-Grassberger formula [28, 31, 36, 37]: $\sum_{\lambda_i > 0} \lambda_i = \kappa + h_{\text{KS}}$, where λ_i s are the Lyapunov exponents of the invariant set, κ is the escape

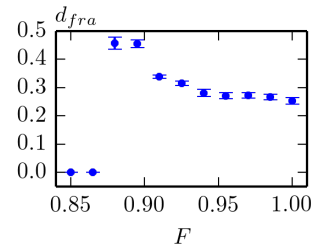


FIG. 5. The abrupt bifurcation observed by varying the force term toward zero. $F = f\tilde{r}_c/E$ is the dimensionless force parameter, where $\tilde{r}_c = |q_m q_e|/\sqrt{mE}$ and E is the total energy of the particle. $F = 1$ corresponds to the original parameter, and $F = 0$ corresponds to the solvable, zero force limit. We can see that the fractal dimension abruptly drops to zero around $F \sim 0.87$.

rate, i.e., $\kappa := \lim_{T \rightarrow \infty} -(1/T) \ln(N(T)/N(0))$ ($N(T)$ is the number of particles remaining in the scattering region at $t = T$), and h_{KS} is the Kolmogorov-Sinai entropy, of which nonzero value implies the chaos. This equation represents the fact that the instability of the invariant set (Lyapunov exponent) leads to two phenomena: The escape of the particle from the scattering region and the growth of the information which is the characteristic feature of the chaos. As we can see, positive λ_i with $h_{\text{KS}} = 0$ is possible because of the finite escape rate κ in contrast to the case with the attractor. For the numerical calculation, the following Young's formula [37, 38] is useful: For the Hamiltonian system with two degrees of freedom, it is $h_{\text{KS}} = \lambda(D_1 - 1)/2$, where D_1 is the information dimension and is defined by

$$D_1 := \lim_{q \rightarrow 1} D_q := \lim_{q \rightarrow 1} \lim_{\delta \rightarrow 0} \frac{1}{q-1} \frac{\log \sum_i p_i^q}{\log \delta}, \quad (5)$$

where δ is the linear size of the box we use to divide the phase space to define the measure p_i , and D_q is the Rényi dimension. Compared to the box counting dimension of the invariant set (D_0), the information dimension reflects the property of the dynamics on the set through the invariant measure p_i .

As is explained above, the information of the saddle which characterizes the chaotic behavior can be understood from the following quantities: κ , λ_i , D_0 , D_1 and h_{KS} . In the following, we calculate characteristic quantities of the fractal peak for $z_0 = -1$ near $x_0 = 0.45$ to confirm that what we found is transient chaos [28].

First, we calculate the uncertainty exponent as follows: We first randomly choose the impact parameter x_0 and $x_0 + \epsilon$ and define that the pair x_0 and $x_0 + \epsilon$ is uncertain if $|t_{\text{pass}}(x_0 + \epsilon) - t_{\text{pass}}(x_0)| > 0.5$ [39]. If t_{pass} has a fractal structure, the number of uncertain pair decays slowly as $\epsilon \rightarrow 0$ compared to the case with the smooth structure: If we denote the fraction of the uncertain pair among all the randomly chosen parameter sets as $F(\epsilon)$,

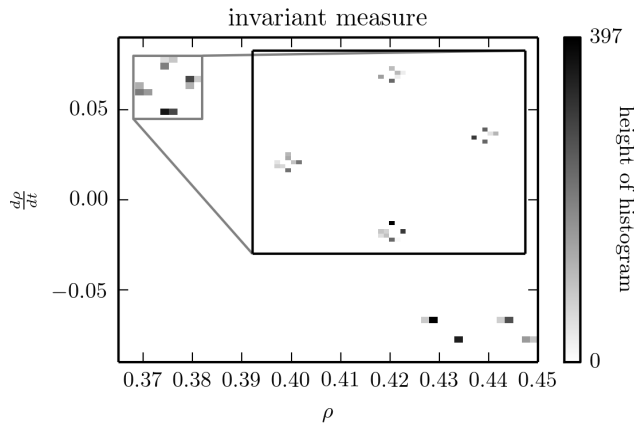


FIG. 6. The invariant measure of the strange saddle on the Poincaré section defined by $z = -0.5r_c$ and $v_z > 0$, obtained by the PIM-triple method [28, 40]. The number of points on Poincaré section obtained from the single trajectory is 3403, and we divide $(\rho, d\rho/dt)$ plane into 50×50 boxes to calculate the histogram. The color represents the height of the histogram, as is shown in the right of the figure.

$F(\epsilon) \sim \epsilon^{d_{\text{unc}}}$ ($\epsilon \rightarrow 0$), and the fractal dimension is given as $d_{\text{fra}} := 1 - d_{\text{unc}} := 1 - \lim_{\epsilon \rightarrow 0} (\ln F(\epsilon) / \ln \epsilon)$. We obtained $d_{\text{fra}} = 0.259 \pm 0.008$. We calculated this exponent for different values of the dimensionless force parameter $F = f\tilde{r}_c/E$, where $\tilde{r}_c = |q_m q_e|/\sqrt{mE}$, with the total energy E fixed. $F = 1$ limit corresponds to the original model Eq. (1) with $\vec{r}(0) = (x_0, 0, -\tilde{r}_c)$ and $\vec{v}(0) = \vec{0}$, while $F = 0$ corresponds to $f = 0$ in Eq. (1) (i.e., the solvable limit [22, 26]) with $\vec{r}(0) = (x_0, 0, -\tilde{r}_c)$ and $\vec{v}(0) = (0, 0, \sqrt{2E/m})$ [26]. We found that the abrupt bifurcation similar to the potential scattering problem [28] occurs around $F \sim 0.87$, see Fig. 5.

Secondly, we calculate the invariant measure of the strange saddle on the Poincaré section defined by $z = -0.5r_c$. We note that our system has two degrees of freedom with the energy conservation, Eq. (3). Accordingly, the dimension of the Poincaré section is two, and we take the coordinate as $(\rho, d\rho/dt)$, where $\rho = \sqrt{x^2 + y^2}$. The result is shown in Fig. 6. From this invariant measure, we can calculate the Rényi dimension D_q in the three dimensional phase space, defined in Eq. (5). We obtain $D_2 = 1.51 \pm 0.02$, $D_1 = 1.52 \pm 0.02$ and $D_0 = 1.54 \pm 0.01$, so D_0 and D_1 are almost the same within the error in our model.

Finally, we calculate the Lyapunov exponent λ and the escape rate κ [26]. We obtained $\lambda = 0.9437 \pm 0.0002$ and $\kappa = 0.676 \pm 0.001$. If we substitute these values to the Kantz-Grassberger formula with Young's formula, we obtain the information dimension of the saddle $D_1 = 1 + 2(1 - \kappa/\lambda) = 1.568 \pm 0.002$, which is in accordance with the result of calculated information dimension of the saddle D_1 . In addition, from Young's formula, we obtain $h_{\text{KS}} = 0.268 \pm 0.001$. Also, the value of D_0 is

consistent with the uncertainty exponent by the formula $D_0 = 1 + 2d_{\text{fra}} = 1.52 \pm 0.02$.

Next, we discuss the stability of the chaotic behavior against the dissipative perturbation [41–43], i.e., $-\eta\vec{r}$ term in the right hand side of Eq. (1). The effect of dissipation on the transient chaos has been studied and is termed as “doubly transient chaos” [44, 45]. The two notable features in their models are as follows [44, 45]: The dissipation leads to the exponential increase of the escape rate, and the fractal dimension decreases monotonically for finer scale ($\epsilon \rightarrow 0$). The former one is in accordance with our model [26], while the latter one is in stark contrast to our model: We found that as we look finer scale, the fractal dimension rapidly grows and saturate at 1 [26]. Since, as is discussed in [44], the decrease of the fractal dimension as increasing the scale is very slow, we speculate that if we look finer scale than 10^{-10} , the fractal dimension eventually decrease. Also we note that this behavior may be due to the peculiarity of our model, i.e., the presence of infinitely many backscattering points. Indeed we observed similar kind of monotonic increase of the fractal dimension in a slightly modified model in the absence of dissipation [26], where we can attribute the increase of the fractal dimension to the infinite number of backscattering points. We note that this behavior strongly depends on the way we regularize the monopole singularity, since r_{min} is very close to zero around the peaks [26]. We also found as we further increase the dissipation, t_{pass} becomes smooth, and the chaos disappears. We further verified the stability against the perturbation which breaks J_z conservation, i.e., the deformation of the mass along x direction. We calculated the fractal dimension and found that it remains finite upon deformation [26]. From these results, we believe that the chaotic behavior we found can be observed in the experiments where the various perturbations exist.

Summary and Discussion. — We found the fractal peak structure in t_{pass} in the scattering problem of a charged particle by magnetic monopole in the presence of a uniform electric field, and verified it is the consequence of the fractal nature of the saddle by calculating the quantities which characterize the saddle. Although our model have a single scatter, i.e., the monopole, the unusual nature of the scattering angle effectively leads to the scattering problem between multiple potential hills. We observed two bifurcation routes (1) by varying the electric field toward zero, where the model is solvable; (2) by introducing the dissipation, through the intermediate region where the fractal dimension monotonically increase as the scale becomes finer. We clarified the stability of the chaotic behavior against the perturbations which exist in the real experiments. In addition to the chaotic scattering, we found that, for small x_0 and $|z_0|$, the particle is captured near the monopole, i.e., t_{pass} diverges. This capturing is caused by the fact that the region which is accessible by the particle is bounded near the monopole,

and we analytically derived the parameter region where the capturing occurs from the form of U_{eff} [26]. Since the semiclassical wave packet passing through the diabolic point in the Born-Oppenheimer energy bands feels the monopole of the Berry curvature and the dynamics of it can be modeled by Eq. (1), the capturing observed here may serve as a mechanism of the bottleneck effect where the relaxation of the excited state toward the ground state is slowed down.

The important future work is the detailed discussion of the symmetry breaking deformation, i.e., the mass deformation. In this case, the system can be characterized by the fast chaotic motion and the slow mode emerged from the small symmetry breaking perturbation. The effect of chaotic classical system on the dynamics of the slow degrees of freedom has been discussed and is termed as the “geometric magnetism” and “deterministic friction” [16, 46]. By extending these notions to the transiently chaotic system with the invariant measure on the saddle [37], it may be possible to discuss the stability of the saddle by examining the fate of the dynamics of the slow degrees of freedom.

The authors thank H. Ishizuka and X. Zhang for useful discussions. This work was supported by JSPS KAKENHI Grant Number JP18J21329 (K.M.), and JSPS KAKENHI Grant Number JP26103006, JP18H03676, and ImPACT Program of Council for Science, Technology and Innovation (Cabinet office, Government of Japan), and JST CREST Grant Numbers JPMJCR16F1, Japan (N.N.).

-
- [1] P. A. M. Dirac, *Proc. R. Soc. Lond. A* **133**, 60 (1931).
 [2] G. 't Hooft, *Nuclear Physics, B* **79**, 276 (1974).
 [3] A. M. Polyakov, *ZhETF Pisma Redaktsiui* **20**, 430 (1974).
 [4] C. Castelnovo, R. Moessner, and S. L. Sondhi, *Nature* **451**, 42 (2008).
 [5] M. V. Berry, *Proc. R. Soc. Lond. A* **392**, 45 (1984).
 [6] J. Dalibard, F. Gerbier, G. Juzeliūnas, and P. Öhberg, *Reviews of Modern Physics* **83**, 1523 (2011).
 [7] N. Goldman, G. Juzeliūnas, P. Öhberg, and I. B. Spielman, *Reports on Progress in Physics* **77**, 126401 (2014).
 [8] P. Zhang, Y. Li, and C. P. Sun, *The European Physical Journal D - Atomic, Molecular, Optical and Plasma Physics* **36**, 229 (2005).
 [9] J. Ruseckas, G. Juzeliūnas, P. Öhberg, and M. Fleischhauer, *Phys. Rev. Lett.* **95**, 010404 (2005).
 [10] M. W. Ray, E. Ruokokoski, S. Kandel, M. Möttönen, and D. Hall, *Nature* **505**, 657 (2014).
 [11] S. Murakami, *New Journal of Physics* **9**, 356 (2007).
 [12] X. Wan, A. M. Turner, A. Vishwanath, and S. Y. Savrasov, *Physical Review B* **83**, 205101 (2011).
 [13] P. Hosur and X. Qi, *Comptes Rendus Physique* **14**, 857 (2013).
 [14] N. P. Armitage, E. J. Mele, and A. Vishwanath, *Reviews of Modern Physics* **90**, 015001 (2018).
 [15] M. Berry and J. Robbins, *Proc. R. Soc. Lond. A* **442**, 641 (1993).
 [16] M. Berry and J. Robbins, *Proc. R. Soc. Lond. A* **442**, 659 (1993).
 [17] G. Sundaram and Q. Niu, *Physical Review B* **59**, 14915 (1999).
 [18] D. Xiao, M.-C. Chang, and Q. Niu, *Reviews of modern physics* **82**, 1959 (2010).
 [19] P. Goddard and D. I. Olive, *Reports on Progress in Physics* **41**, 1357 (1978).
 [20] J. Preskill, *Annual Review of Nuclear and Particle Science* **34**, 461 (1984).
 [21] D. Tong, (2005), arXiv:0509216 [hep-th].
 [22] Y. M. Shnir, *Magnetic Monopoles*, Text and Monographs in Physics (Springer, Berlin/Heidelberg, 2005).
 [23] K. McDonald, “Birkeland, darbox and poincaré: Motion of an electric charge in the field of a magnetic pole (apr. 15, 2015),”.
 [24] G. Darbox, *Bulletin des Sciences Mathématiques et Astronomiques* **2**, 433 (1878).
 [25] H. Poincaré, *Comptes Rendus Acad. Sci* **123**, 530 (1896).
 [26] See supplemental material for the derivation of Eq. (3), the details of the form of U_{eff} and capturing, the origin of the peak structure of t_{pass} , the details of the exact solution of Eq. (1) with $f = 0$, the calculation of the Lyapunov exponent and the escape rate, and the effect of the mass deformation and dissipation.
 [27] P. Gaspard and S. A. Rice, *The Journal of Chemical Physics* **90**, 2225 (1989).
 [28] S. Bleher, C. Grebogi, and E. Ott, *Physica. D, Nonlinear Phenomena* **46**, 87 (1990).
 [29] C. K. Birdsall and A. B. Langdon, *Plasma Physics Via Computer Simulation* (McGraw-Hill, Inc., 1985).
 [30] E. Ott, *Chaos in Dynamical Systems* (Cambridge University Press, 2002).
 [31] Y.-C. Lai and T. Tél, *Transient Chaos* (Springer, 2011).
 [32] D. G. Boulware, L. S. Brown, R. N. Cahn, S. Ellis, and C. Lee, *Physical Review D* **14**, 2708 (1976).
 [33] J. Schwinger, K. A. Milton, W.-Y. Tsai, L. L. DeRaad, and D. C. Clark, *Annals of Physics* **101**, 451 (1976).
 [34] S. Smale, *Bulletin of the American mathematical Society* **73**, 747 (1967).
 [35] Q. Chen, M. Ding, and E. Ott, *Physics Letters A* **145**, 93 (1990).
 [36] H. Kantz and P. Grassberger, *Physica D: Nonlinear Phenomena* **17**, 75 (1985).
 [37] P. Gaspard, *Chaos, scattering and statistical mechanics*, Vol. 9 (Cambridge University Press, 2005).
 [38] L.-S. Young, *Ergodic theory and dynamical systems* **2**, 109 (1982).
 [39] Y.-T. Lau, J. M. Finn, and E. Ott, *Phys. Rev. Lett.* **66**, 978 (1991).
 [40] H. E. Nusse and J. A. Yorke, *Physica D: Nonlinear Phenomena* **36**, 137 (1989).
 [41] A. E. Motter and Y.-C. Lai, *Physical Review E* **65**, 015205 (2001).
 [42] J. M. Seoane, J. Aguirre, M. A. Sanjuán, and Y.-C. Lai, *Chaos: An Interdisciplinary Journal of Nonlinear Science* **16**, 023101 (2006).
 [43] J. M. Seoane, M. A. Sanjuán, and Y.-C. Lai, *Physical Review E* **76**, 016208 (2007).
 [44] A. E. Motter, M. Gruiz, G. Károlyi, and T. Tél, *Phys. Rev. Lett.* **111**, 194101 (2013).
 [45] X. Chen, T. Nishikawa, and A. E. Motter, *Phys. Rev. X*

7, 021040 (2017).

[46] M. V. Berry and E. C. Sinclair, *Journal of Physics A: Mathematical and General* **30**, 2853 (1997).

Supplement material for “Capture and chaotic scattering of a charged particle by magnetic monopole under uniform electric field”

Kou Misaki,¹ Naoto Nagaosa^{1,2}

¹*Department of Applied Physics, The University of Tokyo,
Bunkyo, Tokyo 113-8656, Japan*

²*RIKEN Center for Emergent Matter Science (CEMS),
Wako, Saitama 351-0198, Japan*

Routhian

The Lagrangian describing the charged particle in the presence of the monopole magnetic field can be written as follows:

$$L = \frac{m}{2}(\dot{\rho}^2 + \dot{z}^2 + \rho^2\dot{\phi}^2) - q_m q_e \frac{z}{\sqrt{\rho^2 + z^2}} \dot{\phi} - U(\rho, z), \quad (1)$$

where we assumed that the potential energy U preserves the axial symmetry along z direction, (ρ, ϕ, z) represent the cylindrical coordinates, and the vector potential $A_\phi = -q_m q_e z / \sqrt{\rho^2 + z^2}$ comes from the magnetic monopole at the origin. Since ϕ is the cyclic coordinate of the system, the conjugate momentum

$$J_z = \frac{\partial L}{\partial \dot{\phi}} = m\rho^2 \dot{\phi} - q_m q_e \frac{z}{\sqrt{\rho^2 + z^2}} \quad (2)$$

is conserved. Then, we can construct the Routhian [1]:

$$R = L - J_z \dot{\phi} \Big|_{\dot{\phi} = (J_z + q_m q_e \frac{z}{\sqrt{\rho^2 + z^2}}) / (m\rho^2)} = \frac{m}{2}(\dot{\rho}^2 + \dot{z}^2) - \frac{1}{2m\rho^2} \left(J_z + q_m q_e \frac{z}{\sqrt{z^2 + \rho^2}} \right)^2 - U(\rho, z). \quad (3)$$

As we can see, the dynamics is now described by two degrees of freedom (ρ, z) , and the potential energy is modified to be

$$U_{\text{eff}}(\rho, z) := U(\rho, z) + \frac{1}{2m\rho^2} \left(J_z + q_m q_e \frac{z}{\sqrt{z^2 + \rho^2}} \right)^2. \quad (4)$$

The trapping region of U_{eff}

As is discussed in the main text, if we vary the two parameters (x_0, z_0) , $J_z(x_0, z_0)$ and $E_0(z_0)$ change and for small E_0 and large J_z , the region with $E \leq E_0$ is separated and confined to the finite region, as we can see from Fig. 1(c), thereby leading to the infinite t_{pass} . For smaller J_z , the two regions are connected by the saddle with the energy height $E_{\text{saddle}} < E_0$, leading to finite t_{pass} . To obtain the analytical expression of the boundary between these two cases in (J_z, E_0) plane, we observe that,

$$\begin{aligned} U_{\text{pass}} = E_0 &\Leftrightarrow -Z + \frac{1}{2P^2} \left(\frac{Z}{\sqrt{Z^2 + P^2}} + \tilde{J}_z \right)^2 = \epsilon_0 \\ &\Leftrightarrow 2 \sin v \cos^2 v R^3 + 2\epsilon_0 \cos^2 v R^2 - (\sin v + \tilde{J}_z)^2 = 0, \end{aligned} \quad (5)$$

where $Z := r_c z$, $P := r_c \rho$, $R := r_c r$, $Z = R \sin v$, $P = R \cos v$, $r_c = |q_m q_e|^{2/3} / (mf)^{1/3}$, $\tilde{J}_z := J_z / (q_m q_e)$ and $\epsilon_0 := E_0 / (f r_c)$. The necessary condition for the merger of two separate region is that the discriminant for this third order polynomial for R is zero:

$$\sin^4 v + 2\tilde{J}_z \sin^3 v + (\tilde{J}_z^2 + \alpha) \sin^2 v - \alpha = 0, \quad (6)$$

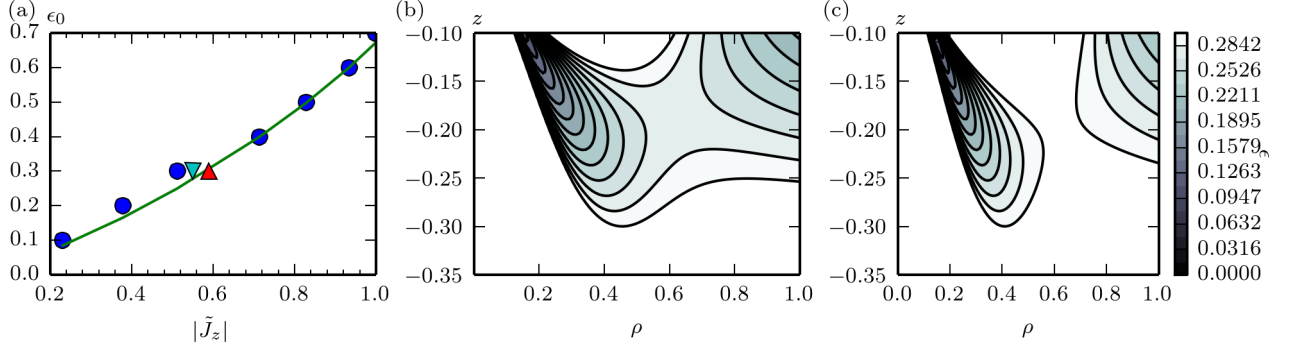


FIG. 1. (a) The boundary separating the trapping orbit and the escaping orbit. The dots are the result of the numerical calculation and the line represents the analytic expression Eq. (8). (b,c) The contour plot for the energy range $0 < \epsilon < \epsilon_0 = 0.3$ and $\tilde{J}_z = 0.55$ and 0.59 for (b) and (c), respectively. The parameter values for (b) and (c) are shown by the blue down triangle and red up triangle in (a), respectively.

where $\alpha := 8\epsilon_0^3/27$. Furthermore, we impose the condition that the discriminant for this fourth order polynomial for $\sin v$ is zero:

$$\alpha^2(\alpha^3 + (3\tilde{J}_z^2 + 8)\alpha^2 + (3\tilde{J}_z^4 - 20\tilde{J}_z^2 + 16)\alpha + \tilde{J}_z^4(\tilde{J}_z^2 - 1)) = 0. \quad (7)$$

Solving this equation for α , we obtain five solutions. Choosing the relevant solution, we obtain

$$\epsilon_0 = \left(-\frac{9}{8}(8 + 3\tilde{J}_z) + \frac{9}{2} \frac{4 + 27\tilde{J}_z^2}{G} + \frac{9}{8}G \right)^{\frac{1}{3}}, \quad (8)$$

where

$$G := \left(64 - 1080\tilde{J}_z^2 - \frac{729\tilde{J}_z^4}{2} + \frac{3\sqrt{3}}{2} \sqrt{\tilde{J}_z^2(-32 + 27\tilde{J}_z^2)^3} \right)^{\frac{1}{3}}. \quad (9)$$

The plot of this curve is shown by the solid line in Fig. 1(a). As a bonus, we obtain the value of J_z where the saddle point of the potential energy vanishes: Above $\tilde{J}_z^2 = 32/27$, the right hand side of Eq. 8 becomes complex, meaning that there is no saddle in the potential energy. Since the chaotic scattering is caused by the pocket of energy minimum bounded by the saddle, we expect no chaotic scattering above this J_z .

Dynamics of charged particle in the presence of monopole

Here, we review the analytic solution in the case of $f = 0$ [2, 3], for completeness. The equation of motion is,

$$m\ddot{\vec{r}} = q_e q_m \frac{\dot{\vec{r}} \times \vec{r}}{r^3}. \quad (10)$$

By taking the inner product with $\dot{\vec{r}}$, and the outer product with \vec{r} , we obtain four conserved quantities:

$$E := \frac{m}{2}(\dot{\vec{r}})^2, \quad \vec{J} := m\vec{r} \times \dot{\vec{r}} - q_e q_m \frac{\vec{r}}{r} =: \vec{L} - q_e q_m \frac{\vec{r}}{r}. \quad (11)$$

Among them, the independent conserved quantities are E , J_z and $|\vec{J}|$. If we take the inner product with \vec{r} and Eq. (10), we obtain $\vec{r} \cdot \ddot{\vec{r}} = 0$, so

$$\frac{d^2 r^2}{dt^2} = 2(\dot{r})^2 = \frac{4E}{m}, \quad \therefore r(t) = \sqrt{(\vec{v}_0)^2 t^2 + 2(\vec{r}_0 \cdot \vec{v}_0)t + (\vec{r}_0)^2} = |\vec{v}_0 t + \vec{r}_0|, \quad (12)$$

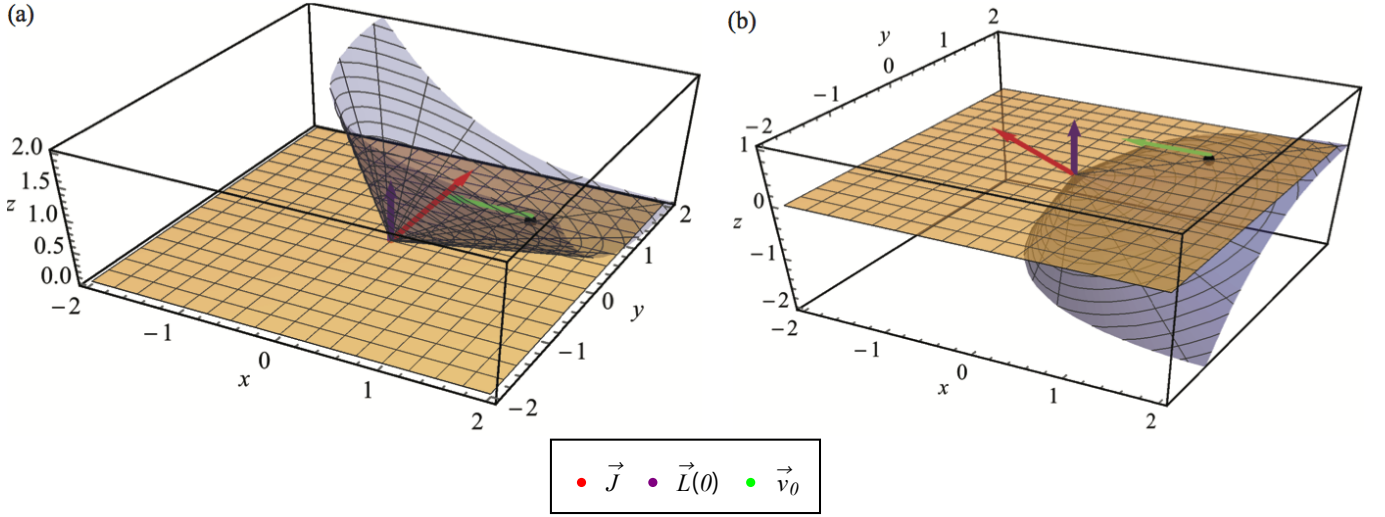


FIG. 2. The cone on which the trajectory of the particle lies (shown blue), in the case of (a) $q_e q_m < 0$ and (b) $q_e q_m > 0$. We can see the direction of the tilting of \vec{J} and the direction of the bending of $x - y$ plane into the cone differ in the two cases. The black dot represents the initial position of the particle, and the red, purple and green arrows represent \vec{J} , $\vec{L}(0)$ and \vec{v}_0 , respectively. We took the z axis along $\vec{L}(0)$ direction, which coincides with \vec{J} in the case of $q_e q_m = 0$, and the orange plane represents $x - y$ plane.

where $\vec{r}(0) = \vec{r}_0$ and $\dot{\vec{r}}(0) = \vec{v}_0$. We assume that \vec{r}_0 is not parallel to \vec{v}_0 . Here, we take \vec{J} along the z direction and take the spherical coordinate (r, θ, ϕ) . Then,

$$\frac{\vec{J} \cdot \vec{r}}{r} = -q_e q_m \Leftrightarrow \cos \theta = \frac{-q_e q_m}{J} = \frac{-q_e q_m}{\sqrt{L^2 + (q_e q_m)^2}}. \quad (13)$$

Finally, we take the inner product of \vec{J} and \vec{L} :

$$\vec{J} \cdot \vec{L} = J^2 - (q_e q_m)^2 \Leftrightarrow L_z = J \sin^2 \theta. \quad (14)$$

Since $L_z = mr^2 \sin^2 \theta \dot{\phi}$, we obtain

$$\dot{\phi} = \frac{J}{mr^2}, \quad \therefore \phi(t) = \frac{1}{\sin \theta} \left[\tan^{-1} \left(\frac{(\vec{v}_0)^2 t + \vec{r}_0 \cdot \vec{v}_0}{|\vec{r}_0 \times \vec{v}_0|} \right) - \tan^{-1} \left(\frac{\vec{r}_0 \cdot \vec{v}_0}{|\vec{r}_0 \times \vec{v}_0|} \right) \right] \quad (15)$$

Combining Eqs. (12), (13) and (15), we obtained the analytical solution. From Eq. (13), we can see that the motion of the particle is restricted on the cone oriented along \vec{J} with the angle $\theta_0 = \cos^{-1}(-q_e q_m/J)$. Here we note that the motion is similar to the motion in the absence of the monopole in two aspects: the motion is restricted to the two dimensional plane (i.e., the cone), and the trajectory on that plane is geodesic. To see the first aspect in more detail, we fix \vec{r}_0 and \vec{v}_0 and show the form of the cone in Fig.2. Here, we let $\vec{L}(0)$ along the z axis to show the difference between $q_e q_m < 0$ and $q_e q_m > 0$ cases (Note the difference of the coordinate system from the analytic solution.). We consider the process where we start from the $q_e q_m = 0$ and gradually increase $|q_e q_m|$. That results in the two modifications: The direction of the total angular momentum tilts toward the position of the particle, \vec{r}_0 , and the surface where the trajectory of the particle lies is bent from the $x - y$ plane into the cone. We note that, since the $x - y$ plane is tangential to the cone at \vec{r}_0 and the initial velocity is along the $x - y$ plane, the particle will not get out of the cone [4]. Since the trajectory of the particle at $q_e q_m = 0$ is the geodesic on the $x - y$ plane, we expect the motion of the particle on the cone is also the geodesic. To verify that this is correct, we define χ as the angle between \vec{r}_0 and \vec{v}_0 . Then,

$$\frac{\vec{r}_0 \cdot \vec{v}_0}{|\vec{r}_0 \times \vec{v}_0|} = \cot \chi = \tan \left(\frac{\pi}{2} - \chi \right), \quad (16)$$

so from Eq. (15),

$$\begin{aligned}
\frac{(\vec{v}_0)^2 t + \vec{r}_0 \cdot \vec{v}_0}{|\vec{r}_0 \times \vec{v}_0|} &= \tan\left(\sin\theta\phi(t) + \frac{\pi}{2} - \chi\right) = -\cot(\sin\theta\phi(t) - \chi) \\
\therefore \frac{(\vec{v}_0)^2 r(t)^2 + (\vec{r}_0 \cdot \vec{v}_0)^2 - (\vec{v}_0)^2 (\vec{r}_0)^2}{|\vec{r}_0 \times \vec{v}_0|^2} &= \cot^2(\sin\theta\phi(t) - \chi) \quad (\because \text{Eq. (12)}) \\
\Leftrightarrow \frac{(\vec{v}_0)^2 r(t)^2}{|\vec{r}_0 \times \vec{v}_0|^2} &= \cot^2(\sin\theta\phi(t) - \chi) + 1 \\
\therefore r(t) \sin(\chi - \sin\theta\phi(t)) &= r_0 \sin\chi. \tag{17}
\end{aligned}$$

To understand this equation, we expand the cone to obtain the development, and consider the two dimensional motion on that. Then, the quantity $\sin\theta\phi(t)$ represents the angle between \vec{r}_0 and $\vec{r}(t)$ in the development of the cone. Since χ represents the angle between \vec{r}_0 and \vec{v}_0 , the above equation can be rewritten as:

$$\vec{v}_0 \cdot \vec{r}(t) = \vec{v}_0 \cdot \vec{r}_0 \quad \text{on the development of the cone.} \tag{18}$$

It means that the motion of the particle is a straight line on the development. In other words, the trajectory is geodesic for the flat metric induced by (locally) identifying the development of the cone with the two dimensional Euclidean space. In this sense, the trajectory is still ‘‘straight’’, although in three dimensional space it looks complicated.

One important feature which is relevant for the main text is Eq. (12). It means that the monopole does not attract the particle to cause the delay of the passing of the particle near the origin.

Hamilton-Jacobi equation

Here we solve $f = 0$ case with the Hamilton-Jacobi method, which may serve as a good starting point for further analysis with the perturbation theory. The Hamiltonian for Eq. (1) obtained by the Legendre transformation is the following:

$$H = \frac{p_r^2}{2m} + \frac{1}{2mr^2} \left[p_\theta^2 + \frac{1}{\sin^2\theta} (p_\phi + q_m q_e \cos\theta)^2 \right]. \tag{19}$$

The Hamilton-Jacobi equation for this Hamiltonian is

$$\frac{\partial S}{\partial t} + H\left(q_i, \frac{\partial S}{\partial q_i}\right) = 0 \Leftrightarrow \frac{\partial S}{\partial t} + \frac{1}{2m} \left(\frac{\partial S}{\partial r}\right)^2 + \frac{1}{2mr^2} \left[\left(\frac{\partial S}{\partial \theta}\right)^2 + \frac{1}{\sin^2\theta} \left(\frac{\partial S}{\partial \phi} + q_m q_e \cos\theta\right)^2 \right] = 0. \tag{20}$$

Since the energy is conserved, ϕ is the cyclic coordinate, and r and θ are separable, we put $S = -\epsilon t + W_r(r) + W_\theta(\theta) + \alpha_\phi \phi$ to obtain

$$\left(\frac{\partial W_\theta}{\partial \theta}\right)^2 + \frac{1}{\sin^2\theta} (\alpha_\phi + q_m q_e \cos\theta)^2 = \alpha_\theta^2 - (q_e q_m)^2, \tag{21}$$

$$\left(\frac{\partial W_r}{\partial r}\right)^2 + \frac{\alpha_\theta^2 - (q_e q_m)^2}{r^2} = 2m\epsilon, \tag{22}$$

where α_θ and α_ϕ corresponds to $|\vec{J}|$ and J_z , respectively. At this point, ϵ , α_θ , and α_ϕ are constants of motion. These equations can be transformed to

$$W_\theta = - \int^\theta d\theta \sqrt{\alpha_\theta^2 - (q_e q_m)^2 - \frac{1}{\sin^2\theta} (q_e q_m \cos\theta + \alpha_\phi)^2}, \tag{23}$$

$$W_r = \int^r dr \sqrt{2m\epsilon - \frac{\alpha_\theta^2 - (q_e q_m)^2}{r^2}}, \tag{24}$$

where we chose the minus sign for W_θ just for convenience. Then, we calculate $\beta_i(q_i, \alpha_i) := \frac{\partial S}{\partial \alpha_i}$, which are canonically conjugate to α_i and are the remaining constants of motion. After a bit long but straightforward calculation, we obtain

$$\beta_\phi := \frac{\partial S}{\partial \alpha_\phi} = \phi - \frac{\pi}{2} + \arctan \left[\frac{\cos A \sin i - \cos i \sin A \sin \psi}{\cos \psi \sin A} \right], \quad (25)$$

$$\beta_\theta := \frac{\partial S}{\partial \alpha_\theta} = \frac{1}{\sin A} \left(\frac{\pi}{2} - \arctan \left[\sqrt{\frac{2m\epsilon r^2}{\alpha_\theta^2 \sin^2 A} - 1} \right] \right) + \psi, \quad (26)$$

$$\beta_0 := \frac{\partial S}{\partial \epsilon} = -t + \sqrt{\frac{m}{2\epsilon}} \sqrt{r^2 - \frac{\alpha_\theta^2 \sin^2 A}{2m\epsilon}}, \quad (27)$$

where

$$\cos \theta = \sin A \sin i \sin \psi + \cos A \cos i, \quad (28)$$

$$\cos A := \frac{-q_e q_m}{\alpha_\theta}, \quad (29)$$

$$\cos i := \frac{\alpha_\phi}{\alpha_\theta}. \quad (30)$$

By solving Eqs. (25), (26) and (27) for (r, ψ, ϕ) , noting that we are free to add $\Delta S(\alpha_i)$ to S to shift each β_i by any function of α_i , we obtain

$$r(t) = \sqrt{\frac{2\epsilon}{m}(t + \beta_0)^2 + \frac{\alpha_\theta^2 \sin^2 A}{2m\epsilon}}, \quad (31)$$

$$\psi(t) = \beta_\theta + \frac{1}{\sin A} \arctan \left[\frac{2\epsilon}{\alpha_\theta \sin A} (t + \beta_0) \right], \quad (32)$$

$$\phi(t) = \beta_\phi - \arctan \left[\frac{\cos A \sin i - \cos i \sin A \sin \psi(t)}{\cos \psi(t) \sin A} \right]. \quad (33)$$

Note that if we substitute

$$\beta_0 = \frac{\vec{v}_0 \cdot \vec{r}_0}{(v_0)^2}, \quad (34)$$

$$\beta_\theta = -\frac{1}{\sin A} \arctan \left[\frac{2\epsilon \beta_0}{\alpha_\theta \sin A} \right], \quad (35)$$

into Eqs. (31) and (32), we reproduce Eqs. (12) and (15).

On the peak structure of t_{pass}

To understand the peak structure of t_{pass} , we consider the following toy model which can be smoothly deformed to our model: We put the potential barrier at $z = -A < 0$ plane, and consider the motion of the particle bouncing back and forth between this potential barrier and the magnetic monopole at the origin. We start from the limit where the barrier is step-like and far from the origin, and smoothly vary the position and thickness of the barrier to reach the limit where the potential can be regarded as the one imitating the uniform electric field.

More concretely, we consider the potential of the form $U(z) = 1 - \tanh((z + A)/B)$, where A represents the position of the wall and B represents the width of the slope of the potential. We set the initial condition as $\vec{v}_0 = \vec{0}$ and $(x_0, y_0, z_0) = (0, 0, -A)$, and calculated $L = |\vec{r} \times \vec{v}|$ and v_z at the first two intersections with the Poincaré section at $z = -A + 1$ with $v_z > 0$. We note that, because of J_z and E conservation, the effective phase space degrees of freedom is three, so the Poincaré map is defined as $(L_n, v_{z,n}) \rightarrow (L_{n+1}, v_{z,n+1})$. We show L_1 , t_{pass} and $\Theta := \arccos(\vec{v}_0 \cdot \vec{v}_1)$ as a function of L_0 in Fig. 3. As we can see, complicated peak structure is observed near the point where $L_0 = L_1$ holds. We note that near these regions, $\Theta \sim 0$, so we speculate that the Poincaré map can be approximated as $(L_n) \rightarrow (L_{n+1})$ at least for this initial regime. By considering the web diagram in Fig. 3(a), we can understand the complicated peak structure of Fig. 3(b): The particles which start from the points sandwiched between the crossing points of blue and black lines goes to smaller L region, and among them, some particles again get to the region

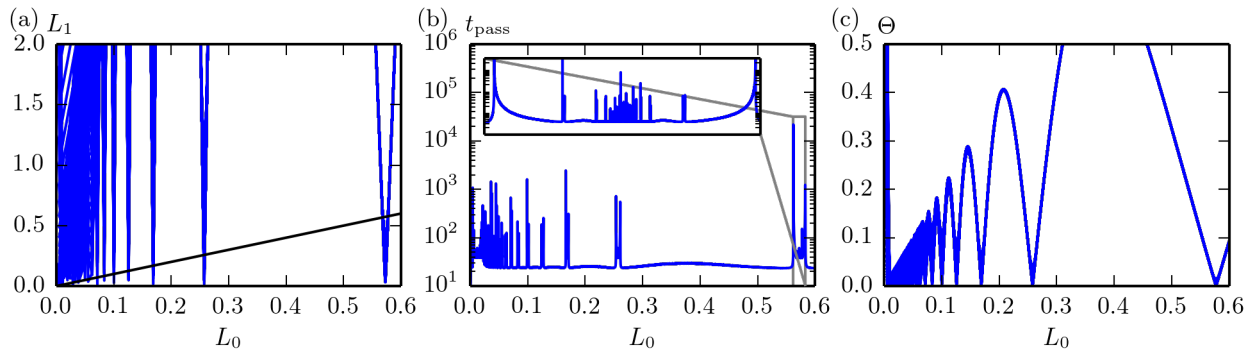


FIG. 3. L_1 , t_{pass} and Θ as a function of L_0 at $A = B = 10$. As we can see, the peak of t_{pass} is near the region where $L_0 = L_1$ holds.

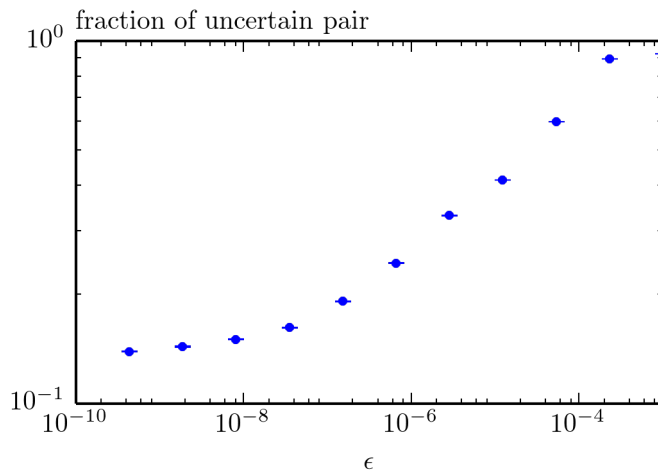


FIG. 4. The fraction of uncertain pair. As we can see, the uncertainty exponent d_{unc} given by the slope (the fractal dimension given by $d_{\text{fra}} = 1 - d_{\text{unc}}$) decreases (increases) as we see finer scale ($\epsilon \rightarrow 0$). The calculation was done for the peak around $L_0 = 0.6$ with $A = B = 10$, see Fig. 3(b).

sandwiched between the crossing points and mapped to smaller L region, and so on. Therefore, we conclude that the complicated peak structure of t_{pass} (Fig. 3(b)) and the monotonic increase of the fractal dimension as a function of scale (Fig. 4) is caused by infinite number of backscattering points, around which L is mapped to smaller value.

As we deform A and B to reach the model which is similar to our model with uniform electric field, these peak structure evolves into the fractal peak, see Fig. 5. So, from the argument above, we speculate that the multiple backscattering points plays the role of the potential hills in the usual chaotic scattering [5, 6], thereby producing the infinite number of symbol sequence by labeling each backscattering points by integers.

The change of U_{eff} from the variation of f

We consider the one parameter family which connects the equation of motion for Eq. (4) where $U(\rho, z) = -fz$ to the one where $U(\rho, z) = 0$, the solvable limit. We define $\tilde{r}_c = |q_m q_e|/\sqrt{mE}$ and $\tilde{t}_c = |q_m q_e|/E$. Then the equation of motion can be rewritten as

$$\begin{cases} \frac{d^2 \tilde{Z}}{d\tilde{\tau}^2} = -\frac{\partial \tilde{U}_{\text{eff}}}{\partial \tilde{Z}} \\ \frac{d^2 \tilde{P}}{d\tilde{\tau}^2} = -\frac{\partial \tilde{U}_{\text{eff}}}{\partial \tilde{P}}, \end{cases} \quad \tilde{U}_{\text{eff}} := -F\tilde{Z} + \frac{1}{2} \left(\frac{J_z}{q_m q_e} + \frac{\tilde{Z}}{\sqrt{\tilde{Z}^2 + \tilde{P}^2}} \right)^2, \quad (36)$$

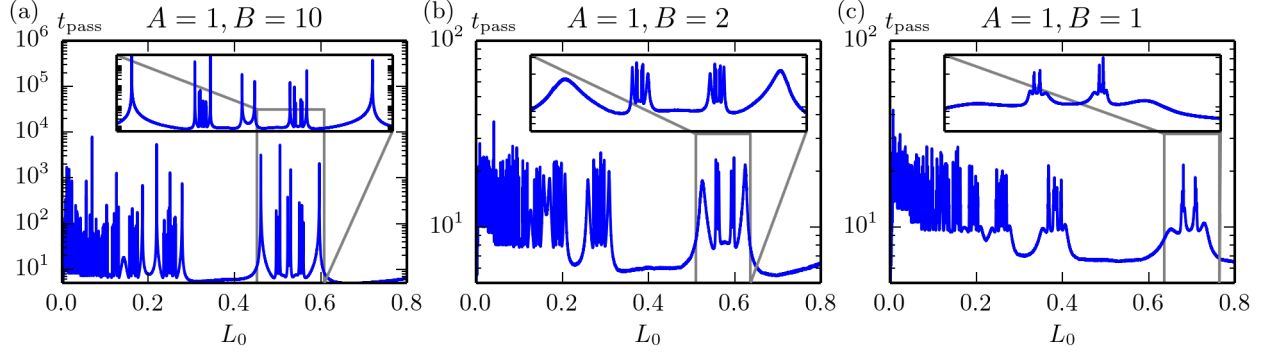


FIG. 5. L_1 , t_{pass} and Θ as a function of L_0 . As we can see, the peak of t_{pass} is near the region where $L_0 = L_1$ holds.

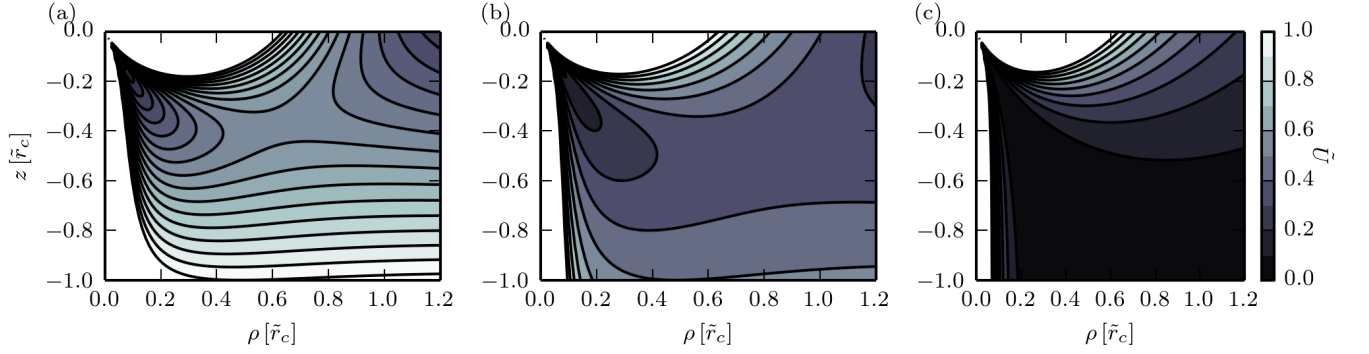


FIG. 6. The change of U_{eff} by varying the dimensionless force parameter, F . Here we set $J_z/(q_m q_e) = 0.9$, and (a) $F = 1$, (b) $F = 0.5$, (c) $F = 0$.

where $\tilde{Z} = z/\tilde{r}_c$, $\tilde{P} = \rho/\tilde{r}_c$, $\tilde{\tau} = t/\tilde{t}_c$ and $F = f\tilde{r}_c/E$. The change of U_{eff} as a function of F is shown in Fig. 6.

The calculation of the Lyapunov exponent and the escape rate

We calculated the Lyapunov exponent from the trajectory obtained by the PIM-triple method, and the escape rate from the time evolution of the number of the surviving particles. The result is shown in Fig. 7. The limiting value of $\chi(t)$ in Fig. 7(a) gives us the Lyapunov exponent, and the slope of the fitting curve (the solid line) in Fig. 7(b) represents the escape rate κ . We note that, since our system is the Hamiltonian system with two degrees of freedom, the energy conservation leads to zero Lyapunov exponent, and the direction of the flow corresponds to another direction with zero Lyapunov exponent. In addition, since the symplectic structure leads to the symmetric distribution of the Lyapunov exponents around zero, the calculation of the one positive Lyapunov exponent is enough.

t_{pass} , r_{min} and the fractal dimension in the presence of the dissipation

We introduced the friction term $-\eta\dot{\vec{r}}$ in our model to quantify the stability of our model against dissipation. We calculated t_{pass} and r_{min} , see Fig. 8. As we can see, upon increasing the amount of the dissipation, the peak structure of t_{pass} drastically changes, and the fractal dimension shows monotonic increase as we see finer scale ($\epsilon \rightarrow 0$), see Fig. 9. As for the escape rate, the time evolution of the number of the surviving particles is similar to the case without dissipation for the short time, i.e., the escape rate is constant (the inset in Fig. 9(b)), while for the long time the escape rate shows monotonic increase, see Fig. 9. This is in accordance with the general behavior in the doubly transient chaos [8, 9]. Note that this behavior is regularization dependent, since r_{min} becomes very close to zero near the peaks upon introducing the dissipation, see Fig. 8(b).

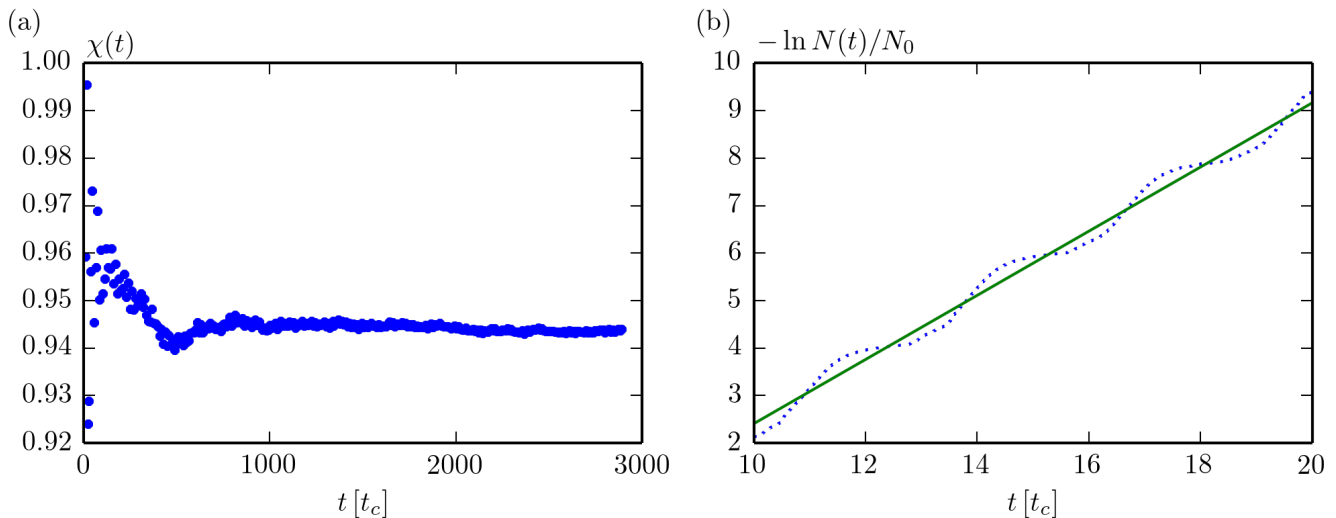


FIG. 7. The calculation of the (a) Lyapunov exponent and (b) escape rate. (a) We calculate $\chi(t)$ by evolving the two nearby phase space points and measure the deviation α_i after the time τ_i to obtain $\chi(t) = (1/\sum_i \tau_i) \sum_i \alpha_i$, of which we obtain the Lyapunov exponent from the limiting value [6, 7]. (b) The dotted line represents the numerically obtained number of surviving particles as a function of time, and the solid line is the fitting curve. The slope of the curve is the escape rate.

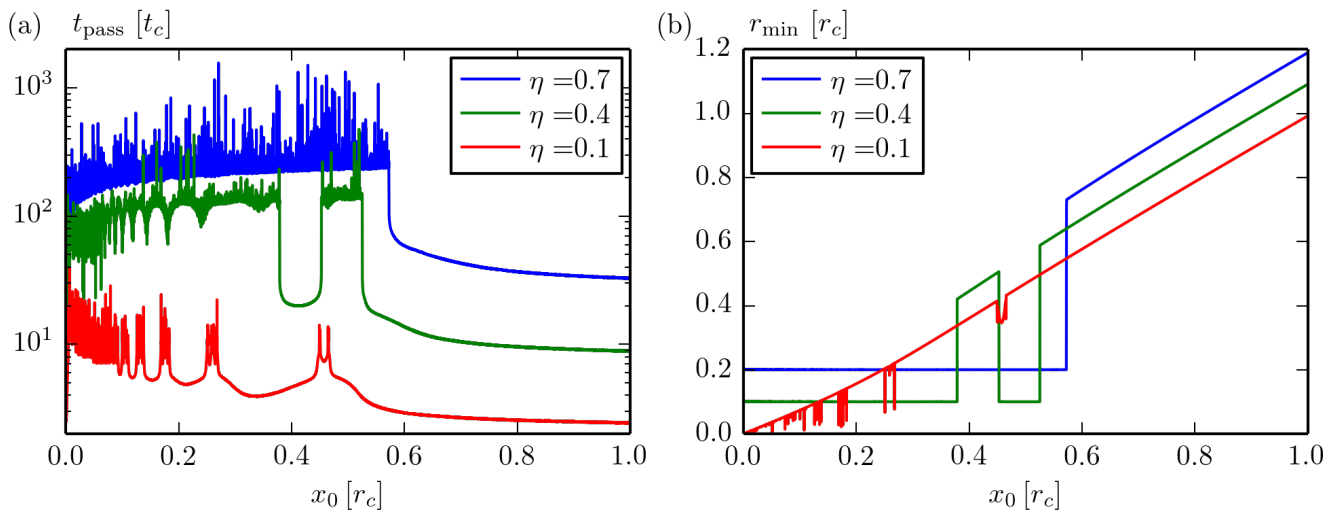


FIG. 8. The plots of the (a) t_{pass} and (b) r_{min} . The value of η is shown above (a). As we can see, as we increase the strength of the dissipation, the fractal peak becomes broad with rapid variation and r_{min} is very close to zero, which means that this behavior strongly depends on the way we regularize the monopole singularity. Note that the plots are shifted upward.

Stability against the mass deformation

Since the rotational symmetry along z direction leads to the reduction of one degree of freedom, it is important to verify the stability against the deformation which breaks the symmetry. We calculated the variation of the fractal dimension under increasing the mass along x direction, see Fig. 10. As we can see, the fractal dimension remains positive against the finite amount of the perturbation, and then becomes zero. Therefore, we expect our result is valid even in the realistic situation where the rotational symmetry along z direction is broken.

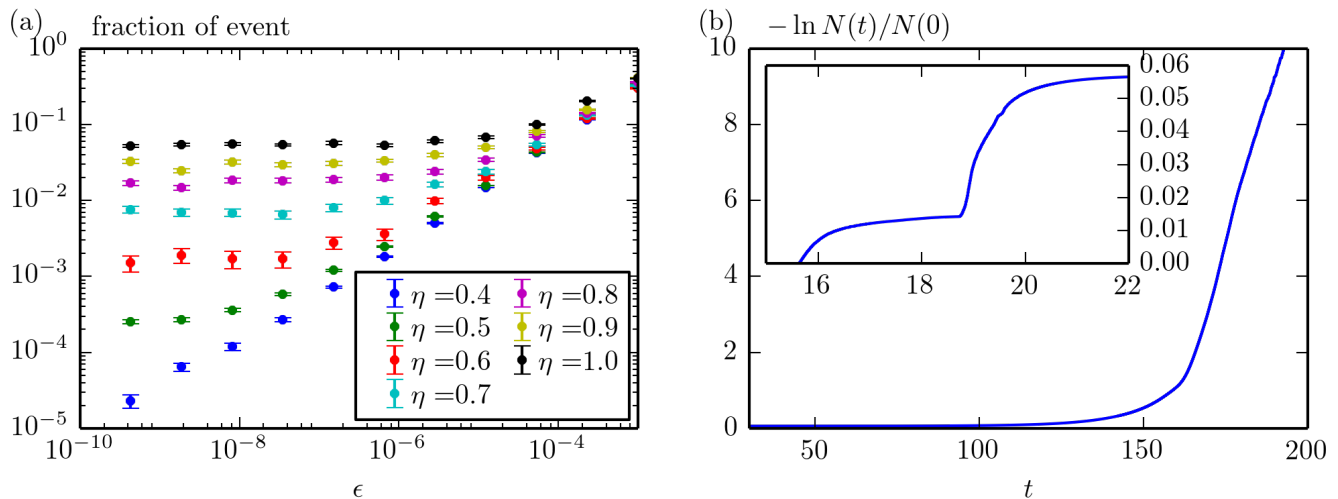


FIG. 9. The plots of the (a) fraction of uncertain pair, and (b) the minus logarithm of the number of surviving particles. (a) As we can see, the uncertainty exponent d_{unc} given by the slope in (a) (the fractal dimension given by $d_{\text{fra}} = 1 - d_{\text{unc}}$) decreases (increases) as we see finer scale ($\epsilon \rightarrow 0$), which is in stark contrast to the doubly transient chaos. The value of η is as is shown in the legend. (b) The inset shows the early time behavior, which shows linear behavior in time. After some time (around $t = 100$), the number of escaping particles suddenly increases, which means the monotonic increase of the escape rate.

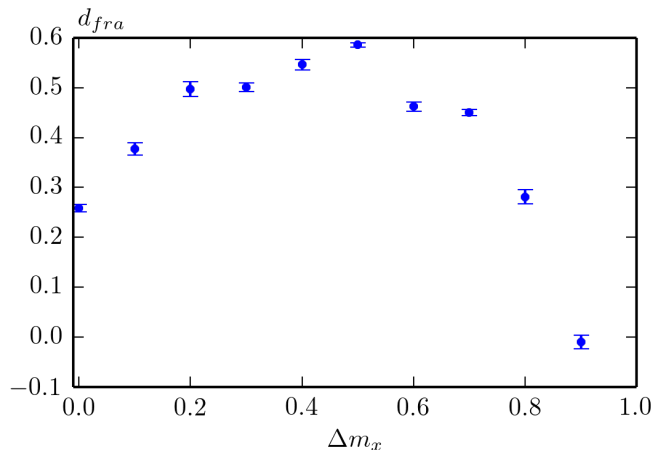


FIG. 10. The fractal dimension against the mass deformation, Δm_x . $\Delta m_x = m_x - 1$ and $\Delta m_x = 0$ is the original parameter. By increasing Δm_x , the mass along x direction becomes large and the system becomes more and more anisotropic.

-
- [1] H. Goldstein, C. Poole, and J. Safko, *Classical mechanics* (2002).
[2] G. Darboux, *Bulletin des Sciences Mathématiques et Astronomiques* **2**, 433 (1878).
[3] H. Poincaré, *Comptes Rendus Acad. Sci* **123**, 530 (1896).
[4] In other words, once the direction of \vec{J} is fixed from Eq. (11), then the opening angle is automatically determined from the requirement that the cone should be tangential to the plane subtended by the vectors \vec{r}_0 and \vec{v}_0 .
[5] P. Gaspard and S. A. Rice, *The Journal of Chemical Physics* **90**, 2225 (1989).
[6] S. Bleher, C. Grebogi, and E. Ott, *Physica. D, Nonlinear Phenomena* **46**, 87 (1990).
[7] E. Ott, *Chaos in Dynamical Systems* (Cambridge University Press, 2002).
[8] A. E. Motter, M. Gruiz, G. Károlyi, and T. Tél, *Phys. Rev. Lett.* **111**, 194101 (2013).
[9] X. Chen, T. Nishikawa, and A. E. Motter, *Phys. Rev. X* **7**, 021040 (2017).